Volume 282, number 2, 247–252 FEBS 09663 May 1991

ADONIS 001457939100371P

Conformation of sarafotoxin-6b in aqueous solution determined by NMR spectroscopy and distance geometry

Robyn G. Mills[1], Annette R. Atkins[2], Tim Harvey[1], F. Keith Junius[1], Ross Smith[2] and Glenn F. King[1]

[1] *Department of Biochemistry, University of Sydney, NSW 2006, Australia,* [2] *Department of Biochemistry, University of Queensland, Qld 4072, Australia* and [3] *Department of Biochemistry, University of Oxford, Oxford, OX1 3QU, UK*

Received 9 January 1991; revised version received 20 February 1991

The solution structure of sarafotoxin-6b in water has been determined using high-resolution NMR spectroscopy. 127 proton–proton distance measurements and three φ dihedral angle constraints derived from NMR spectra were used to calculate the solution structure using a combination of distance geometry and restrained molecular dynamics. The major structural feature of the resulting family of five structures was a right-handed α-helix extending from K9 to Q17. In contrast, the C-terminal region of the peptide appears not to adopt a preferred conformation in aqueous solution. The present structure is compared with those previously determined for endothelin peptides in non-aqueous solvents.

Sarafotoxin; Endothelin; NMR; Protein Structure; Bronchoconstriction; Distance Geometry

1. INTRODUCTION

The sarafotoxins are a group of 4 peptide toxins first isolated in 1982 from the venom of the Israeli burrowing asp, *Atractaspis engaddensis* [1,2]. These 21-residue peptides show remarkable sequence homology to the recently discovered endothelins, to date the most potent endogenous vasoconstrictors in mammalian vasculature [3].

Together, these peptides form a newly defined family of vaso- and bronchoconstrictors, all of which evoke similar physiological responses by binding to a unique group of receptors. The primary physiological effect, peripheral vasoconstriction, is generally believed to result from a polyphosphoinositide-mediated increase of intracellular Ca^{2+} in vascular smooth muscle cells [3].

Correspondence address: G.F. King, Department of Biochemistry, The University of Sydney, Sydney NSW 2006, Australia. Fax: (61) (2) 692-4571.

Abbreviations: NMR, nuclear magnetic resonance; ET-1, endothelin-1; DMSO, dimethylsulphoxide; S6b, sarafotoxin-6b; DG, distance geometry; RMD, restrained molecular dynamics; CD, circular dichroism; FID, free induction decay; TPPI, time proportional phase incrementation; 2D HOHAHA, two-dimensional homonuclear Hartmann Hahn spectroscopy; 2D DQF-COSY, two-dimensional double quantum filtered correlated spectroscopy; rf, radio-frequency; 2D NOESY, two-dimensional nuclear Overhauser effect spectroscopy; τ_m, mixing period in NOESY experiment; τ_c, temperature relaxation time of bath; Δ_t, time step; K_{dc}, force constant for NMR restraints; αCH, α-carbon proton; NH, amide proton; βCH, β-carbon proton; RMSD, root mean square deviation; nOe, nuclear Overhauser effect

Chemical modifications of endothelin [4] and sarafotoxin [5], such as destruction of one or both disulphide bridges, cleavage of the intramolecular loop by lysyl endopeptidase, or removal/modification of the C-terminal Trp, all lower vasoconstrictive potency with respect to the native peptide. This suggests that these structural features are essential for vasoconstrictive activity.

Recent NMR studies of endothelin-1 (ET-1) in non-physiological solvents such as DMSO or acetic acid/water mixtures have identified an irregular helix between residues K9 and C15 (e.g. [6–9]). However, whilst Saudek et al. [6,10] propose that the region from H16 to W21 is closely associated with the N-terminal portion of ET-1, Endo et al. [7] concluded that the C-terminal tail does not adopt a defined conformation.

We present here a preliminary *aqueous* solution structure of S6b, the most potent of the sarafotoxins; we believe this to be the first structure of a member of the endothelin/sarafotoxin family which has been determined in pure water solvent. The structure of S6b was determined by using distance and torsion angle constraints derived from ^{1}H-NMR experiments in conjunction with distance geometry (DG) and restrained molecular dynamics (RMD) calculations.

2. MATERIALS AND METHODS

2.1. *Materials*

5 mg of sarafotoxin S6b (amino acid sequence = CSCKDMTDKECLYFCHQDVIW) was obtained from the American Peptide Co. (Santa Clara, CA). Tetramethylsilane was from Aldrich Chemical Co. (Milwaukee, WI). All other reagents were analytical grade. The DG program, DISMAN was kindly provided by Dr.

Werner Braun (Institute of Molecular Biology and Biophysics, Zurich). The RMD program, GROMOS, was from BIOMOS (University of Groningen, The Netherlands).

2.2. *CD experiments*

Circular dichroism (CD) spectra were recorded on a Jobin Yvon (Roussel-Jouan, France) Dichrographe III that had been calibrated at 304 nm against an epiandrosterone standard. A 2 nm bandpass was used with a time constant of 20 s and a pathlength of 1 mm. The peptide was dissolved in water at a concentration of 0.39 mM and adjusted to the desired pH by the addition of NaOH. Blank spectra were recorded with water only in the optical cell. Mean residue ellipticities were calculated using a mean residue molecular weight of 122.1, based on a peptide molecular weight of 2564.

2.3. *NMR experiments*

S6b was dissolved in a mixture of 95% H_2O/5% D_2O to give a final concentration of 3.9 mM, and 1 mM sodium azide was added. Experiments were conducted on the sample at pH 3.6 and 310K, and pH 3.1 and 303K. Dilute HCl and NaOH were used to adjust the pH.

A high resolution one-dimensional (1D) NMR spectrum was collected at pH 3.1, 303K for the measurement of $^3J_{NH_N CH}$ coupling constants. 128 summed FIDs were collected in 16 000 data points. Prior to Fourier transformation, the time domain was zero-filled once and multiplied by a Lorentz-Gaussian function. The final digital resolution was ~0.21 Hz/pt.

Two-dimensional (2D) NMR spectra were recorded in phase-sensitive mode using the TPPI method [11] on Bruker AMX-400 wide-bore and AMX-600 narrow-bore spectrometers. Spectra acquired on these spectrometers had similar signal-to-noise ratios (~330:1) as a dedicated proton probe was available for the AMX-400 spectrometer whilst for the AMX-600 spectrometer, proton experiments were performed with an inverse probe which ultimately failed to meet signal-to-noise specifications. The spectral widths were 4800 and 6600 Hz at 400 and 600 MHz, respectively. The sample was not spun in any experiment.

The raw data for each 2D experiment consisted of 480–512 FIDs, each consisting of 64–144 scans into 4000 complex data points. Generally, zero-filling and shifted sine bell apodization were employed in each dimension prior to Fourier transformation. However, some NOESY spectra were apodized using a Lorentz-Gauss function in the real-time dimension. Typically, the final dimensions of the 2D spectra were 4000 × 1000 real data points. Baselines were corrected using a third order polynomial function.

The spin-lock in 2D HOHAHA experiments, which was obtained using a MLEV-17 pulse sequence [12], had an rf field strength of ~6 kHz. The trim pulses were 2.5 ms. Continuous saturation of the water resonance was performed during the relaxation time (1.5 s) in all experiments and additionally during the mixing periods in NOESY and HOHAHA spectra.

Sequence-specific resonance assignments and proton-proton distance constraints were derived from 2D NOESY experiments. The presence of crosspeaks resulting from spin diffusion was assessed by following the build-up of crosspeak intensity in NOESY spectra obtained with mixing periods (τ_m) ranging from 200–500 ms. After eliminating crosspeaks arising from spin-diffusion, proton-proton distance constraints were derived from crosspeak intensities in a 2D NOESY spectrum with τ_m = 350 ms; this NOESY represented a suitable compromise between reasonable crosspeak intensity and minimal spin diffusion effects.

2.4. *Calculation of solution structure*

Dipolar couplings were classified into the following 3 groups of upper distance constraints according to their intensity level as judged by counting contour levels: 2.8 Å (strong), 3.3 Å (medium), and 4.5 Å (weak). In addition, the ϕ torsion angles were constrained to the range −90° to −30° for $^3J_{NH_N CH} \leq 5.1$ Hz. The disulphide bridges, C1–C15 and C3–C11, were fixed in the DG calculations by constraining the S–S distance to an upper limit of 2.1 Å and the S–βC distances across each bridge to an upper limit of 3.1 Å [13].

Using the DISMAN program on a Silicon Graphics IRIS 4D workstation, 50 DG structures were calculated from random starting conformations using 127 upper distance constraints and three ϕ angle constraints. Nine structures, selected on the basis of their final penalty function values, were then chosen for further refinement. This involved 200 steps of steepest restrained energy minimisation, followed by

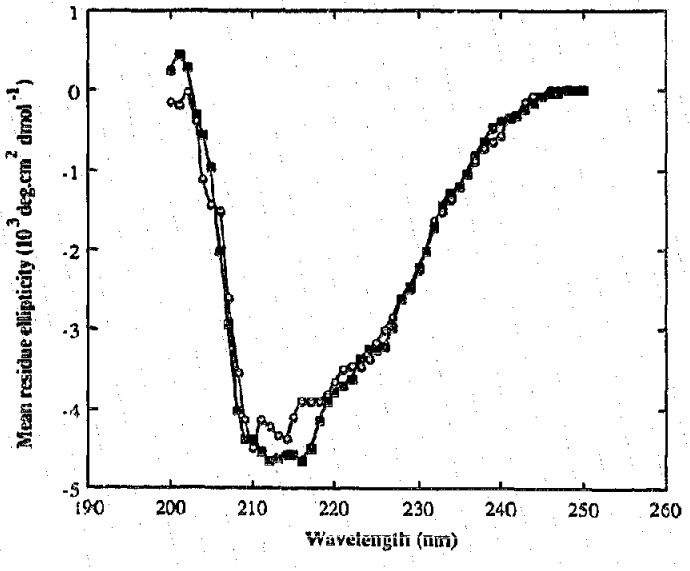

Fig. 1. CD spectra of S6b in H_2O at pH 3.6 (■) and pH 7.5 (○); note the similarity of the spectra collected at these different pH values. The shoulder in both spectra at ~223 nm is indicative of α-helical secondary structure.

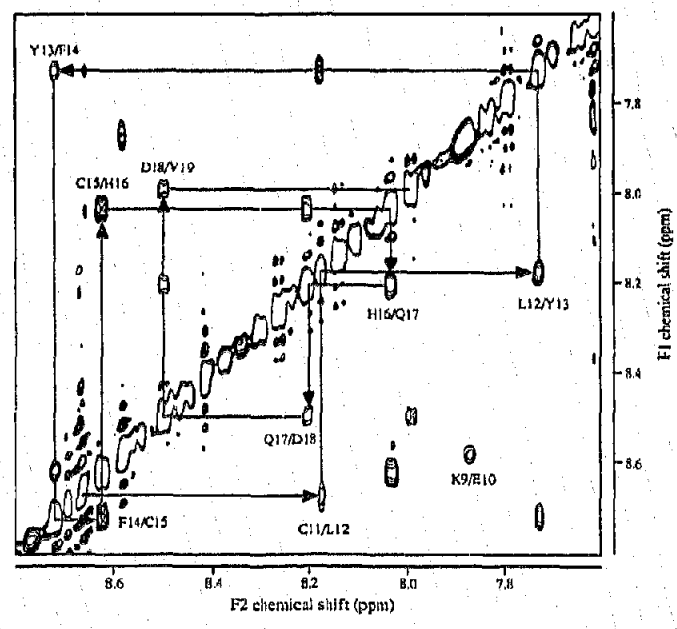

Fig. 2. A portion of 2D NOESY spectrum (τ_m = 350 ms) of S6b (3.9 mM, pH 3.1, 303K) showing sequential NH–NH connectivities (i.e. connectivities between the backbone amide protons of neighbouring residues). The arrowed lines trace out the connectivities from C11 to V19. The weak dipolar coupling between E10 and C11 can only be seen in contour plots containing lower-intensity contour levels.

Table 1

Proton resonance assignments for sarafotoxin-6b at pH 3.1, 303K[a]

Residue	NH	αCH	βCH	β'CH	γCH	γ'CH	γCH3	γ'CH3	δCH	δ'CH	δCH3	δ'CH3	εCH
C1		4.23	3.34	3.13									
S2	8.94	4.74	3.87										
C3	8.78	4.96	3.40	2.96									
K4	8.07	4.15	1.72		1.40	1.33							2.99
D5	8.86	4.55	3.16	2.89									
M6	7.92	4.10	2.20	1.88	2.50	2.43							
T7	7.96	4.45	4.63				1.34						
D8	8.84	4.45	2.92										
K9	8.44	3.99	1.86	1.77	1.54	1.41			1.70				3.01
E10	7.73	4.16	2.23		2.64	2.58							
C11	8.53	4.63	3.19										
L12	8.03	4.03	1.77	1.57	1.69						0.86	0.83	
C15	8.48	4.77	3.20	2.91									
Q17	8.06	4.32	2.10	1.94	2.28								
D18	8.35	4.67	2.90	2.74									
V19	7.85	4.04	1.86				0.77	0.65					
I20	8.00	4.16	1.79		1.38	1.10	0.83				0.81		

Residue	NH	αCH	βCH	β'CH	2H	2,6H	3,5H	4H	5H	6H	7H	NH
Y13	7.58	4.25	3.06	3.00		6.83	6.75					
F14	8.58	4.31	3.22	3.09		7.37	7.50	7.41				
H16	7.89	4.63	3.36	3.34	8.53			7.23				
W21	8.13	4.71	3.37	3.23	7.24			7.65	7.18	7.22	7.46	10.03

[a]Chemical shifts are referenced to internal tetramethylsilane at 0.00 ppm

20 ps of RMD refinement [14]. The system was equilibrated for 4 ps at 900K by coupling to a 900K temperature bath [15] with a temperature relaxation time (τ_c) of 0.01 ps. The force constant for NMR restraints (K_{de}) was 20 000 kJ · mol^{-1} · nm^{-2} and the time step (Δt) was 2 fs, with all bond lengths being kept rigid using the SHAKE algorithm [16]. This was followed by 4 ps of RMD at 900K with τ_c = 0.1 ps. Over the next 6 ps, the system was cooled by coupling to a bath at 300K (τ_c = 1.0 ps). The system was then maintained at 300K for 10 ps (τ_c = 0.1 ps) with K_{de} set at 1000 kJ · mol^{-1} · nm^{-2}.

The conformations during the last 5 ps of RMD were averaged and minimised with restraints to provide the final structures for this study. Graphical analysis of DG-derived structures was performed using the MidasPlus suite of programs (University of California, San Francisco).

3. RESULTS

The biological activity of the S6b sample was confirmed by assay of bronchoconstrictive activity in isolated human bronchus; it was fond in this assay to induce a mean maximal contractile response significantly greater than that induced by ET-1 and ET-2 (previously published data; [17]).

The similarity of CD spectra of S6b at pH 3.6 and pH 7.4 (Fig. 1) indicates that the gross conformation of the peptide in aqueous solution is unaltered between physiological pH (7.4) and the acidic pH (3.6) required for NMR observation of labile amide protons. Furthermore, the shoulder observed at ~223 nm in both CD spectra is indicative of a component of α-helix in the native solution structure of S6b.

The unique spin systems of M6, T7, L12, V19 and I20 could be sequence-specifically assigned in all 2D HOHAHA and DQF-COSY spectra, whereas assignment of the remaining spin systems, of which 12 were AMX-type, required the combined results of spectra collected at both pH/temperature conditions. This was necessitated by the unusually large number of α-carbon protons, resonating close to the frequency of solvent water. By shifting the water resonance (which chemical shift is both pH- and temperature-dependent) downfield, it was possible to assign all αCH resonances. Furthermore, there were fewer degenerate NH resonances at pH 3.1, 303K, which proved essential for unequivocal assignment of nOe crosspeaks involving NH resonances. Sequential NH–NH connectivities

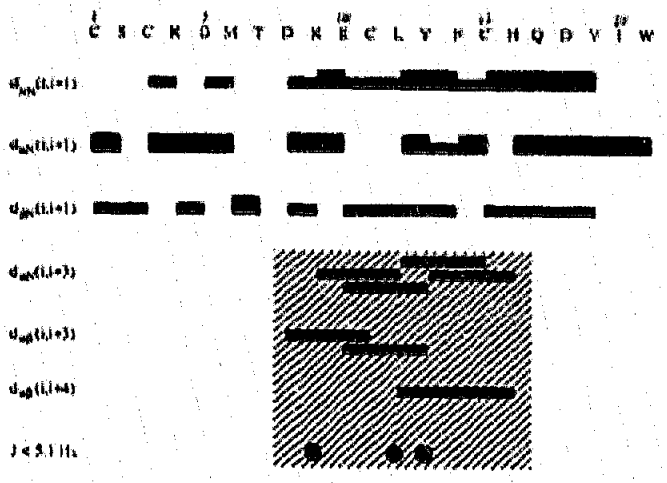

Fig. 3. Summary of the inter-residue nOe connectivities and low $J_{NH\alpha CH}$ values observed for S6b in this study. The solid bars indicate the presence of an nOe and the height of the bar is proportional to the nOe intensity. The hatched area highlights nOe connectivities and $J_{NH\alpha CH}$ values indicative of an α-helix.

between residues 8 and 19 (Figs 2 and 3) and sequential αCH-NH connectivities between residues 12 and 21 enabled the unequivocal sequence-specific assignment of all resonances in the segment 8-21. In the segment 1-7, K4 and D5 were then assigned through a process of elimination. The remaining spin systems, C1 and C3, were discriminated by the presence of sequential NH-NH as well as αCH-NH connectivities between residues 3 and 6, and sequential βCH-NH connectivities.

All resonances were assigned for S6b at pH 3.1, 303K and the chemical shifts are given in Table I. A summary of observed nOes is given in Fig. 3. Inspection of this fugure reveals not only a stretch of sequential NH-NH connectivities between residues 8 and 19, which is characteristic of helices, but also a large number of medium range connectivities (i.e. $d_{i,i+3}$, $d_{i,i+4}$) and low values of $J_{NH\alpha CH}$ in this region, which are more specifically indicative of α-helices. Complete analysis of NOESY spectra yielded a total of 127 structurally im-

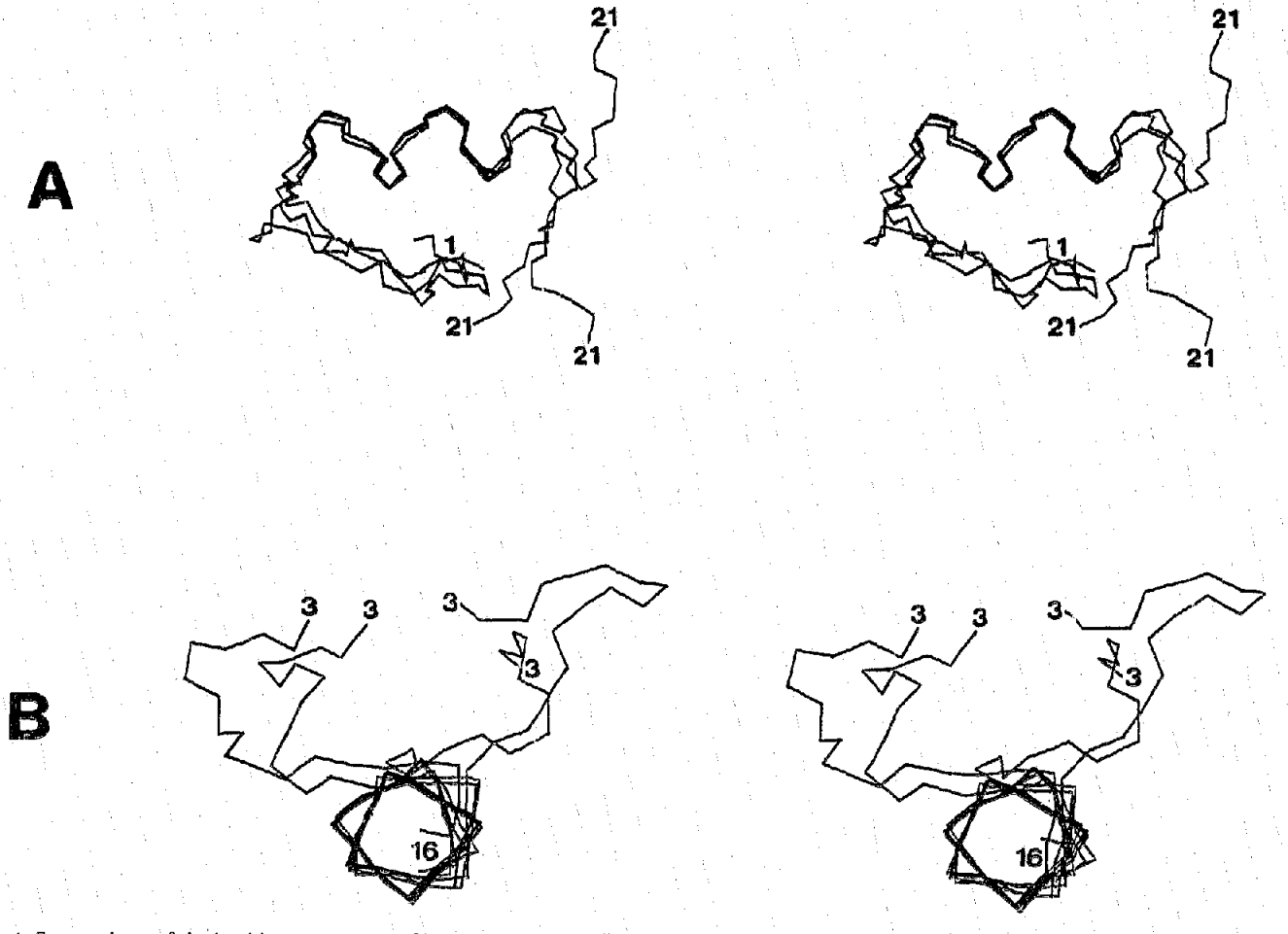

Fig. 4. Stereo views of the backbone atoms (N, C, αC, O) of the family of solution structures of S6b obtained from combined DG/RMD calculations: (a) a view showing all residues from three of the final five structures (two are omitted for clarity) superimposed for minimum RMSD over the region K9-Q17; (b) four of the family of structures (residues 3–16 only) viewed down the long axis of the helical region. This view illustrates the two sub-families of structures which satisfy the present NMR constraints.

portant dipolar-couplings which were used in the DG and RMD calculations: 69 intra-residue, 48 sequential and 10 medium-range. The ϕ dihedral angles of K9, L12, and Y13 were restrained to the range $-30°$ to $-90°$ in these calculations based on their low values of $J_{NH_N CH}$ (< 5.1 Hz).

A family of 5 structures resulted from the combined DG and RMD calculations (see Fig. 4a,b). The major structural feature of the peptide is a well-defined right-handed α-helix extending from K9 to Q17 (average RMSD for the backbone atoms over this segment = 0.44 Å); Fig. 5 shows that the ϕ and ψ angles of the family of structures converge to $-60°$ in this region. The occurrence of specific $C{=}O_i$ to NH_{i+4} hydrogen bonds was estimated as the percentage of time for which a particular bond was present during the last 5 ps of the RMD trajectory [18], averaged over the entire family of structures. The backbone amide protons of residues 12–18 were found to be involved in specific hydrogen bonds of this type for >60% of the time, which agrees with preliminary amide temperature coefficient data obtained on the peptide (to be published elsewhere).

Examination of the overlaid structures (Fig. 4) reveals two sub-families differentiated by the direction in which the polypeptide chain travels after exiting from the N-terminal end of the α-helix. This is highlighted in Fig. 4b, which shows a view looking down the long axis of the helical region of the overlaid structures. Examination of Fig. 5 indicates that this variation is largely caused by variation in the sign of the ϕ angle at T7. It remains to be seen whether this variation in the loop region of the peptide is due to conformational flexibility or a lack of NMR constraints; stereospecific assignments, especially of the cysteinyl βCH_2s, may help to decide this issue.

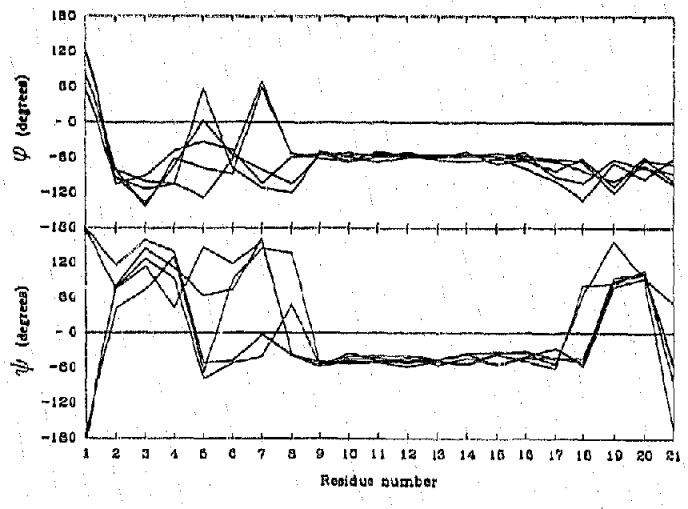

Fig. 5. Phi (ϕ) and psi (ψ) angles for each residue in the final 5 structures resulting from the combined DG/RMD calculations. For residues between K9 and Q17 inclusive, there is strong convergence of both the ϕ and ψ angles to $-60°$, which is characteristic of α helix. Note, however, the divergent ϕ angles for T7, which seem to be largely responsible for the divergent paths the backbones of the two families of structures take after exiting from the N-terminal end of the α-helix.

The DG and RMD calculations reveal that C-terminal tail of S6b (D18–W21) appears to have no well-defined conformation in aqueous solution, consistent with the few nOe constraints obtained from this region. (As a result, the average RMSD for the backbone atoms over the entire molecule is 3.53 Å.) However, there are some short-range dipolar interactions between the side-chains of V19, I20, and W21 and the downfield shifting of one of the V-19 γ-methyl protons is presumably due to ring-current shift effects arising from proximity to the W21 indole ring. Hence, there may be local hydrophobic interactions involving the three C-terminal residues.

4. DISCUSSION

The present study has revealed a regular right-handed α-helix in S6b extending from K9 to Q17. Previous NMR studies of endothelin in non-physiological solvents have also revealed helical stretches; however, these have usually involved fewer residues, ranging from K9–C15 for ET-1 in DMSO [6,7] and ET-3 in 10% acetic acid [8] to K9–H16 for ET-1 in 40% acetic acid [9]. Furthermore, all of the helical regions reported for ET-1 and T-3 in these non-physiological solvents are irregular and far removed from being standard right-handed α-helices. It is unlikely that these discrepancies with the present structure represent intrinsic conformational differences between the solution structures of S6b and ET-1/ET-3 since the amino acid sequences of these peptides are identical in the region K9–H16. More likely is that the helices in the NMR-determined ET structures are distorted due to the nature of the solvents used in these studies or because the structures (with the exception of those in [6]) have not been fully refined using RMD.

The present study failed to find evidence of any interaction between the C-terminus of S6b and the N-terminal portion of the peptide. This concurs with all previous NMR studies on ET peptides except those by Saudek's group on ET-1 [6,10] and ET-3 [8] in DMSO. Determination of the solution structure of a member of the endothelin family in pure water solvent may help to decide whether this discrepancy is due to the non-aqueous solvent used in these studies or the result of better nOe data collected by the Saudek group.

In summary, we have determined the structure of S6b in aqueous solution and consequently believe it to be the best representation thus far of the biologically active conformation of a member of the endothelin/sarafotoxin family. The structure needs to be further refined before attempts can be made to correlate conformational features of the peptide with its biological activity. With this in mind, we are currently attempting

to improve the quality of the family of solution structures by making stereospecific NMR assignments and measuring temperature coefficients for the backbone amide protons.

Acknowledgements: We thank the Australian National Heart Foundation and the University of Queensland for financial support, Ms. Karen McKay for assays of S6b activity, and Dr. Vladimir Saudek for providing manuscripts prior to publication.

REFERENCES

[1] Takasaki, C., Tamiya, N., Bdolah, A., Wollberg, Z. and Kochva, E. (1988) Toxicon 26, 543–548.
[2] Bdolah, A., Wollberg, Z., Fleminger, G. and Kochva, E. (1989) FEBS Lett. 256, 1–3.
[3] Yanagisawa, M. and Masaki, T. (1989) Biochem. Pharm. 38, 1877–1883.
[4] Kimura, S., Kasuya, Y., Sawamura, T., Shinmi, O., Sugita, Y., Yanagisawa, M., Goto, K. and Masaki, T. (1988) Biochem. Biophys. Res. Commun. 156, 1182–1186.
[5] Kitazumi, K., Shiba, T., Nishiki, K., Furukawa, Y., Takasaki, C. and Tasaka, K. (1990) FEBS Lett. 260, 269–272.
[6] Saudek, V., Hoflack, J. and Pelton, J.T. (1990) Int. J. Pept. Prot. Res., in press.
[7] Endo, S., Inooka, H., Ishibashi, Y., Kitada, C., Mizuta, E. and Fujino, M. (1989) FEBS Lett. 257, 149–154.
[8] Bertmann, P., Hoflack, J., Pelton, J.T. and Saudek, V. (1990) Neurochem. Int., in press.
[9] Dalgarno, D.C., Senior, M.M., Slater, L.B. and Chackalamannil, S. (1990) Proc. XIVth Int. Conf. Magn. Reson. Biol. Systems, P8–7.
[10] Saudek, V., Hoflack, J. and Pelton, J.T. (1989) FEBS Lett. 257, 145–148.
[11] Wüthrich, K. (1988) Science 243, 45–50.
[12] Bax, A. and Davis, D.G. (1985) J. Magn. Res. 65, 355–360.
[13] Williamson, M.P., Havel, T.F. and Wuthrich, K. (1985) J. Mol. Biol. 182, 295–315.
[14] Van Gunsteren, W.F. and Berendsen, H.J.C. (1987) Groningen Molecular Simulation (GROMOS) Library Manual, Biomos, Nijenbourgh 16, Groningen, The Netherlands.
[15] Ryckaert, J.P., Ciccotti, G. and Berendsen, H.J.C. (1977) J. Comp. Physics 23, 327–341.
[16] Van Gunsteren, W.F. and Berendsen, H.J.C. (1977) Mol. Phys. 34, 1311–1327.
[17] Mills, R.G., McKay, K., Atkins, A.R., Smith, R., Black, J. and King, G.F. (1990) Proc. Aust. Biochem. Soc. 22, SP85.
[18] Pastore, A., Harvey, T.S., Dempsey, C.E. and Campbell, I.D. (1989) Eur. Biophys. J. 16, 363–367.